



# **Geophysical Research Letters**\*



# **RESEARCH LETTER**

10.1029/2022GL098457

#### **Key Points:**

- Observations support kinetic Alfvén waves (KAWs) as the acceleration mechanism for auroral beads
- KAWs were generated around the equator where local plasma convection matched beads' azimuthal motion
- KAW accelerated electrons were observed and further Alfvénic acceleration might occur down to 2
   Re altitude

#### **Supporting Information:**

Supporting Information may be found in the online version of this article.

#### Correspondence to:

S. Tian, tianx138@umn.edu

#### Citation:

Tian, S., Lyons, L. R., Nishimura, Y., Wygant, J. R., Lysak, R. L., Ferradas, C. P., et al. (2022). Auroral beads in conjunction with kinetic Alfvén waves in the equatorial inner-magnetosphere. *Geophysical Research Letters*, 49, e2022GL098457. https://doi.org/10.1029/2022GL098457

Received 22 MAR 2022 Accepted 21 APR 2022

© 2022. The Authors.

This is an open access article under the terms of the Creative Commons Attribution-NonCommercial-NoDerivs License, which permits use and distribution in any medium, provided the original work is properly cited, the use is non-commercial and no modifications or adaptations are made.

# Auroral Beads in Conjunction With Kinetic Alfvén Waves in the Equatorial Inner-Magnetosphere

S. Tian<sup>1,2</sup> , L. R. Lyons<sup>2</sup> , Y. Nishimura<sup>3</sup> , J. R. Wygant<sup>1</sup> , R. L. Lysak<sup>1</sup> , C. P. Ferradas<sup>4,5</sup> , X. An<sup>6</sup>, A. B. Igl<sup>1,7</sup>, G. D. Reeves<sup>4</sup>, B. A. Larsen<sup>4</sup> , and D. Ma<sup>2</sup>

<sup>1</sup>School of Physics and Astronomy, University of Minnesota, Minneapolis, MN, USA, <sup>2</sup>Department of Atmospheric and Oceanic Sciences, University of California, Los Angeles, CA, USA, <sup>3</sup>Department of Electrical and Computer Engineering and Center for Space Physics, Boston University, Boston, MA, USA, <sup>4</sup>Los Alamos National Laboratory, Los Alamos, NM, USA, <sup>5</sup>Geospace Physics Laboratory, NASA Goddard Space Flight Center, Greenbelt, MD, USA, <sup>6</sup>Department of Earth, Planetary, and Space Sciences, University of California, Los Angeles, CA, USA, <sup>7</sup>Department of Physics and Astronomy, Louisiana State University, Baton Rouge, LA, USA

**Abstract** Auroral beads are spatially wavy forms routinely seen before the onset of auroral substorms and are closely related to the onset-related instabilities. To date, the acceleration mechanism of electrons that create auroral beads is not fully determined. Here, we present a fortuitous event when the Van Allen Probe A (RBSP-A) was in magnetic conjunction with auroral beads. RBSP-A observed Alfvén waves, locally generated kinetic Alfvén waves (KAWs) and Alfvénic accelerated electrons at several 100 eV. The Alfvén waves and KAWs carried sufficient Poynting flux to power visible aurora and may control the beads' motion. These observations and previous simulations support that the Alfvénic acceleration is the acceleration mechanism of the auroral beads. Specifically, KAWs are generated around the equator and accelerate local cold electrons to several 100 eV. The waves are suggested to propagate to both hemispheres and accelerate electrons to several keV, which directly account for the auroral beads.

Plain Language Summary Auroral display in the ionosphere is part of a complicated energy release process called the geomagnetic substorm. During substorms, auroral beads, a type of spatially wavy aurora, appear and then suddenly brighten and expand in local time and latitude. Because auroral beads are routinely seen before the sudden brightening and expansion, they are widely studied to understand why aurora evolves in such an explosive way. To date, it is generally accepted that auroral beads map to a source region in the equatorial plasma in space where waves and plasma instabilities occur. It is also known that the auroral beads are directly caused by electrons of keV energy precipitating into the ionosphere. However, how these electrons are accelerated along the magnetic field lines from the source region to the ionosphere is unknown. Here, we analyze the wave and plasma data measured by the Van Allen Probe A satellite when auroral beads occurred. We find that a type of low frequency wave, called the kinetic Alfvén wave, is generated within the source region and can accelerate local electrons to several 100 eV energy and can potentially further accelerate these electrons to keV to trigger auroral beads.

# 1. Introduction

Auroral beads are spatially wavy auroral forms along the equatorward arc (Akasofu, 1964; Elphinstone et al., 1995; Henderson, 1994). They often develop to auroral substorms (Donovan et al., 2006; Henderson, 2009; Liang et al., 2008; Rae et al., 2010) but may also develop into pseudo-breakups or occur during non-substorm times (Xing et al., 2020). Pseudo-breakups can be considered as an intermediate condition between the non-substorm time and a standard substorm. Statistical studies show that auroral beads are seen for >90% onsets of auroral substorms (Kalmoni et al., 2017; Nishimura et al., 2016). This means that the first signature of the auroral substorm is the initiation of beading. Thus, understanding the physics of beading is crucial to understanding how and when substorms occur.

Much progress has been made on understanding the spatial and temporal evolution of the auroral beads based on optical observations. For example, auroral beads are seen to develop symmetrically in both hemispheres (Motoba et al., 2012), which paints a clear physical connection between beads and a source region in the equatorial magnetosphere. The wavelength of the beads typically ranges from 30 to 150 km in the ionosphere (Kalmoni et al., 2015; Nishimura et al., 2016). The beads are typically observed around 22 hr MLT and may propagate

TIAN ET AL 1 of 9



eastward, or westward, or in both directions, at a speed of 2–6 km/s in the ionosphere (Nishimura et al., 2016). These observations, if compared to the wave observations at the source region, would significantly improve our understanding of beading physics. Recent THEMIS studies have studied regions around the source region for tailward driver (Panov et al., 2019) and plasma convection (Nishimura et al., 2022). However, no comparisons between beads and waves in the source region have been reported.

The intensity of beads grows exponentially, suggesting a certain instability develops in the source region (Kalmoni et al., 2017; Nishimura et al., 2016; Rae et al., 2010). Many instabilities have been proposed to cause beading, including the shear flow ballooning instability (Viñas & Madden, 1986; Voronkov et al., 1997), kinetic ballooning instability (Cheng & Lui, 1998), kinetic ballooning interchange instability (Pritchett & Coroniti, 2010), and cross field current instability (Lui et al., 1991). So far, observational studies on instabilities related to beads are primarily based on optical analysis (Rae et al., 2010; Rae & Watt, 2016; Kalmoni et al., 2015, 2017, 2018; Nishimura et al., 2016. Yet there is no scientific consensus on which instability causes beading. Direct observations around the source region would help to resolve which instability corresponds to beading.

Besides the physical connection between beads and the source region, another important open question is the acceleration mechanism of electrons that create auroral beads. At low-altitudes (<1,000 km), spacecraft in conjunction with beads observed keV electrons accelerated by both the quasi-static potential drop and Alfvén waves (Motoba & Hirahara, 2016). Fourier analysis based on the optical signatures suggests that the dispersion relation of beads resembles that of kinetic Alfvén waves (KAWs; Kalmoni et al., 2018). Although KAWs have been viewed as a probable candidate, determining which acceleration mechanism is operating along the flux tubes of the beads requires direct in-situ observations.

In this study, we present a fortuitous event when auroral beads were in magnetic conjunction with the Van Allen Probe A (RBSP-A) around the equatorial magnetosphere. We analyze the in-situ electromagnetic waves and local plasma status to identify the acceleration mechanism of the auroral beads, compare the wave properties to the optical signatures of the beads, and place constraints on beading instabilities. In the rest of the paper, we introduce the relevant instrumentation in Section 2, and present and discuss the observations in Section 3 and Section 4. The conclusions are listed in Section 5.

# 2. Instrumentation

Onboard RBSP-A, the DC magnetic fields are measured by the EMFISIS instrument (Kletzing et al., 2013) at 64 samples/sec, and the DC electric fields are measured by the EFW instrument (Wygant et al., 2013) at 32 samples/sec in the spin plane. The magnetic field  $\vec{B}$  is decomposed into the background ( $\vec{B}_0$ ) and wave ( $d\vec{B}$ ) magnetic fields. The background magnetic field is obtained by filtering below 0.5 mHz. The spin axis electric field is not well measured in DC and thus we calculate it from the commonly used  $\vec{E} \cdot \vec{B}_0 = 0$  assumption. For KAWs, although  $E_{\parallel}$  is non-zero, it is much smaller than  $E_{\perp}$  because  $k_{\perp} \gg k_{\parallel}$ . Therefore the  $\vec{E} \cdot \vec{B}_0 = 0$  assumption is approximately valid for KAWs. The electric and wave magnetic fields are downsampled to 16 samples/sec to calculate the 3D Poynting flux. The local plasma properties are provided by the HOPE instrument (Funsten et al., 2013), which measures electrons and ions (H+, He+, and O+) from several eV to 50 keV per charge. The HOPE cadence is 22 s, providing moments including the density, bulk velocity, and temperature for each species. We use the moments of the dominant ion species (H+ and O+) to estimate the needed plasma parameters, for example, the number density ratio of O+ ( $r_0$ ) and the MHD bulk velocity ( $\vec{v}$ ). In conjunction with the RBSP-A, the THEMIS all-sky imager (ASI; Mende et al., 2008) at GBAY (Goose Bay) records auroral images every 3 s at a typical spatial resolution of 1 deg, enabling us to resolve auroral beads and their spatial and temporal evolution.

# 3. Observations

Figure 1 shows the overall observations over 9 hr around the Feb 18, 2015 event. The event occurred around 02:10 UT when auroral beads were observed by the all-sky imager at GBAY (Goose Bay) and in conjunction with RBSP-A (Panel f). The wavelength of the auroral beads around 02:10 UT was about 140 km at 110 km altitude, which falls into the typical range of 30–150 km (Kalmoni et al., 2015; Nishimura et al., 2016). This wavelength scales to  $\theta_b = 2.8$  deg (Panel f), or 1,745 km at the radial distance of RBSP-A. A movie of the development of the auroral beads is attached in Supporting Information S1. As shown in the movie, the auroral beads developed

TIAN ET AL 2 of 9

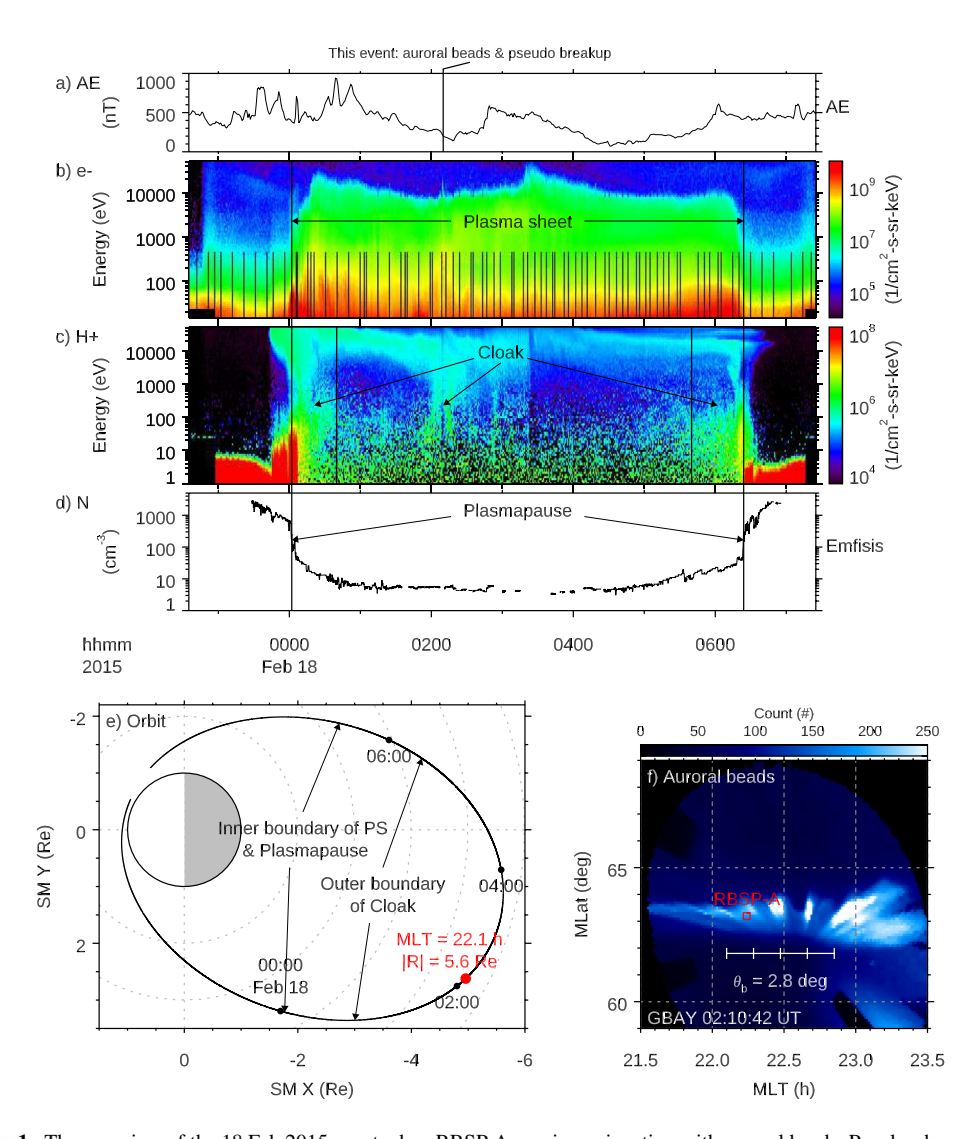


Figure 1. The overview of the 18 Feb 2015 event when RBSP-A was in conjunction with auroral beads. Panel a shows the AE index and the time of the event is marked by the vertical line. Panels b and c show the electron and H+ energy spectrogram over an entire orbit of RBSP-A, showing the entry and exit of the plasma sheet around the vertical lines at 00:02 and 06:24 UT. The location of the entry and exit of the plasma sheet are marked by the arrows in Panel e. In addition, Panel c shows the times when the plasma cloak was observed. Panel d shows the total electron density derived from the EMFISIS upper-hybrid line. The vertical lines coincide with the plasmapause crossings in the outbound and inbound portions of the orbit. In Panel e, the locations of the boundaries of the plasma sheet, plasmapause, and plasma cloak are marked along the orbit of RBSP-A in the equatorial plane. Panel f shows a snapshot of the auroral beads, the footpoint of RBSP-A (red), and the wavelength of the beads ( $\theta_b \sim 2.8$  deg, or 140 km at the ionosphere).

into a pseudo-breakup, because there was no substantial poleward expansion or AE increase. Note that despite not developing into a full substorm, the beading characteristics seen around 02:10 UT are the same as the beading that is seen for a full substorm (Kalmoni et al., 2015; Nishimura et al., 2016). This indicates that the beading physics is the same. Thus this event is appropriate for giving information on what drives the beading in general, including for a full substorm.

Panels b and c show the electron and H+ energy spectrum measured by the HOPE instrument. The vertical lines mark the entry and exit times of the plasma sheet, which is characterized by the existence of keV electrons. These boundaries coincided with the plasmapause, as seen in the density derived from the upper hybrid line from the EMFISIS measurement (Panel e). In addition, Panel c shows that the plasma cloak, which contains H+ warmer than the plasmasphere (Chappell, 1982), was observed outside the plasmapause and encountered around the time of the conjunction event. The spacecraft orbit and the aforementioned boundaries are marked in Panel e. During

TIAN ET AL 3 of 9



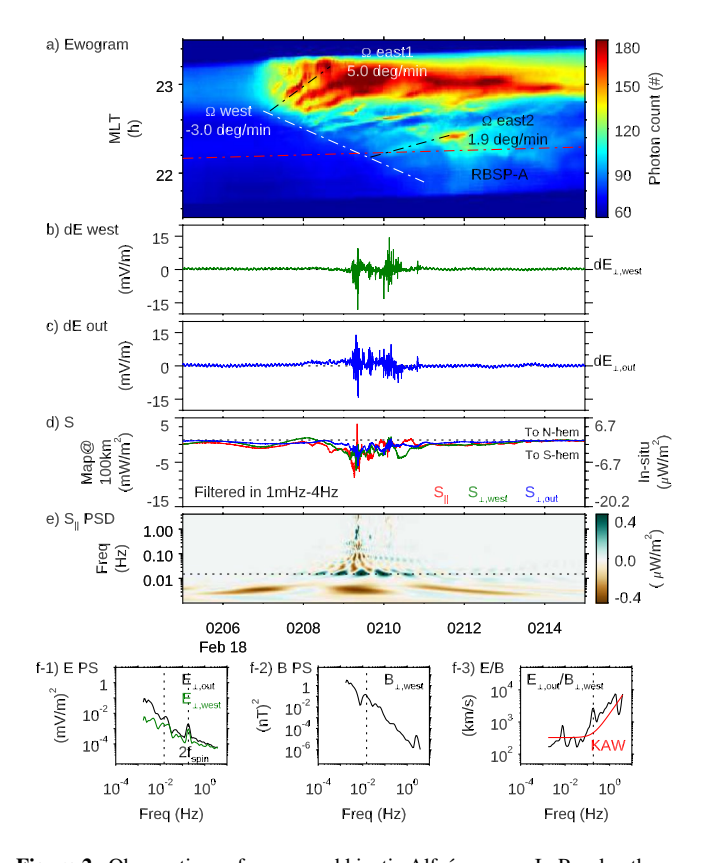


Figure 2. Observations of aurora and kinetic Alfvén waves. In Panel a, the auroral beads drifted eastward at 1.9-5.0 deg/min (black lines). The overall envelope expanded westward at 3 deg/min (white line), meeting the local time of RBSP-A (red line) around 02:09 to 02:10 UT. Around this time, RBSP-A observed strong wave activities (Panels b and c) and significant parallel Poynting flux (Panel d). Panels b and c show the electric field along the westward (toroidal) and outward (poloidal) components in the field-aligned coordinate. The other component, the electric field along the magnetic field, is essentially 0 and thus not shown. Panel d shows the 3D Poynting flux. Panel e shows the power distribution of the parallel Poynting flux in the time-frequency domain. The dashed line marks a northward Poynting flux around 0.015 Hz. Panels f-1 and f-2 show the power spectrum of the electric and magnetic fields. Spectral peaks are seen around 0.015 Hz and also at  $2f_{spin}$ in Panel f-1. Panel f-3 shows the E/B ratio as a function of frequency (black) and the expected dispersion relation for kinetic Alfvén waves (red). To directly compare to Equation 1, the E/B ratio is calculated using  $E_{\perp,out}$  and  $B_{\perp,west}$ 

this orbit, the plasmasphere and the plasma sheet contacted around 3.3–3.5 Re, and the plasma cloak extended to 4.3–4.5 Re. Around the time of the conjunction, the plasma cloak reappeared around 5.6 Re. It was also seen at a similar MLT in the previous orbit (not shown), suggesting that the plasma cloak was associated with a spatial structure. This will be further discussed later in this section.

Figure 2 shows the auroral ewogram and the DC wave observations over 10 min around the conjunction. Individual auroral beads, moving eastward in local time, are noticed as stripes in the ewogram (Panel a). The eastward motion ranged from 1.9 to 5.0 deg/min based on manual estimation. These angular speeds scale to 1.6–4.2 km/s, consistent with statistical values (Nishimura et al., 2016). On the other hand, the overall extent of the auroral beads expanded westward around 3 deg/min (Panel a), passing the local time of RBSP-A around 02:09 to 02:10 UT. Around this time, RBSP-A observed significant parallel Poynting flux toward the southern hemisphere  $(|S_{\parallel}| > 10 \text{ mW/m}^2 \text{ when normalized to } 100 \text{ km altitude, } \text{Panel d}) \text{ associated}$ with strong electric field fluctuations (>10 mV/m, Panels b and c). The southward Poynting flux is expected as RBSP-A was below the magnetic equator (negative  $B_{0x}$ , Table 1). Since existing observations revealed that auroral beads develop symmetrically in conjugate hemispheres (Motoba et al., 2012), we suppose that similar Poynting fluxes might propagate toward both hemispheres. Note that although the total parallel Poynting flux was primarily southward (Panel d), its frequency-time spectrogram (Panel e) shows that there are northward Poynting fluxes at some frequencies, for example, around 0.015 Hz (dotted line). Both the northward and southward Poynting fluxes are unidirectional and thus correspond to traveling waves. The direction change in frequency has been observed in other auroral events (Tian et al., 2021), but the reason for the direction change is unclear.

The electric field fluctuations are identified as KAWs because the E/B ratio of the measured waves is consistent with that of KAW (Panel f-3). According to Chaston et al. (2014), the dispersion relationship of KAW (Lysak & Lotko, 1996) can be expressed in terms of the spacecraft frequency  $f_{SC}$  as

$$\frac{E_{\perp,out}}{B_{\perp,west}} = \frac{B_0}{\sqrt{\mu_0 m_i n}} \sqrt{1 + \frac{f_{SC}^2}{f_{gi}^2} \frac{v_i^2}{v_{\perp mest}^2}},\tag{1}$$

where  $B_0$ ,  $m_i$ , n,  $f_{gi}$ ,  $v_i$ , and  $v_{\perp,west}$  are the magnitude of the magnetic field, average ion mass, plasma density, ion cyclotron frequency, ion thermal speed, and azimuthal flow speed in the SC frame, respectively. The values of these quantities are obtained based on RBSP-A measurement and are listed

in Table 1. In this study, vectors are expressed in a field-aligned coordinate, where the three axes are along  $\vec{B}_0$ , westward, and outward directions. The latter two components are both perpendicular to  $\vec{B}_0$ . Equation 1 assumes  $\omega_{SC} = 2\pi f_{SC} \sim \vec{k} \cdot \vec{v}$ , where  $\omega_{SC}$  and  $\vec{k}$  are the angular frequency and wave vector. According to Table 1, the dominant component of  $\vec{v}$  is  $v_{\perp,west}$ . Thus the latter is used in Equation 1 for simplicity.

In Panel f-3, the measured E/B ratio (black) is calculated from the frequency spectra of  $E_{\perp,out}$  and  $B_{\perp,west}$  (Panels f-1 and f-2). The calculation is over the frequency range from 1.67 mHz to 4 Hz, corresponding to the duration of the data (600 s) and the sampling rate (16 Samples/sec). The measured E/B ratio plateaued around the Alfvén speed  $v_A$  below 0.1 Hz ( $\ll f_{gi} = 3.8$  Hz, Table 1), suggesting that these low frequency waves are Alfvén waves. Above 0.1 Hz, the measured E/B ratio gradually increased from  $v_A$  and followed the expected KAW dispersion relationship (red). The peak around 0.2 Hz is instrumental, arising from the electric field (Panels f-1 and f-3). From these observations, we conclude that the observed waves consist of Alfvén waves and KAWs. Based on the expected dispersion relationship, the transition occurred around 0.1–0.2 Hz. KAWs can be generated from Alfvén

TIAN ET AL 4 of 9

1-1.5



Table 1		
The Values of Parameters Related to the In-Situ Plasma and Auroral Beads Around 02:10 UT		
Parameter	Value	Note
n	5.5 cm <sup>-3</sup>	Plasma number density from EMFISIS upper hybrid frequency
$r_{O}$	18%	$r_O = n_O/(n_O + n_H)$ , $n_O$ and $n_H$ are partial densities (>50 eV)
$B_0$	70 nT	Background magnetic field $\vec{B}_0 \sim (-40, 9, 57)  \mathrm{nT}$ in solar magnetic coordinates
$m_i$	$3.7m_H$	Averaged ion mass, $m_i = \sum_s r_s m_s$ , where $s = H$ , $O$ and $r_H = 1 - r_O$
$f_{gi}$	3.8 Hz	Ion cyclotron frequency, $f_{gi} = eB_0/m_i$
$v_i$	477 km/s	Ion thermal speed, $v_i = \sum_s r_s v T_s$ , where $v_{Ts} = \sqrt{T_s/m_s}$
v	27 km/s	MHD flow speed, $\vec{v} = (13, -20, 11)$ km/s, along $\vec{B}_0$ , west, and out directions
$v_A$	340 km/s	Alfvén speed, $v_A = B_0 / \sqrt{\mu_0 n m_i}$
$r_{SC}$	5.6 Re	RBSP-A distance to Earth
MLat	-0.4 deg	RBSP-A magnetic latitude
MLT	22.1 hr	RBSP-A magnetic local time
$\theta_b$	2.8 deg	Wavelength of beads in angle, or 140 km at ionosphere

waves through energy cascade and/or phase mixing (Génot et al., 2004; Wright et al., 1999). Note that the power spectrum of  $E_{\perp,out}$  is larger than  $E_{\perp,west}$ , especially at low frequencies (<0.01 Hz, Panel f-1). Therefore using  $E_{\perp,out}$  here captures the main power of the electric field.

Plasma beta (for plasma up to 50 keV)

Figure 3 shows the plasma observations over the 10 min around the time of the auroral beads and kinetic Alfvén waves. RBSP-A observed electrons in the 100–400 eV energy range (Panel b, around 02:09 to 02:10 UT). Pitch angle distributions show that these electrons are beams along the background magnetic field (Panels a-2 to a-4), whereas the electron distribution was isotropic before the event (Panel a-1). In Panel c, a density increase around 02:09 to 02:10 UT is evidenced in both the EFW density, which is obtained by fitting the spacecraft potential to the EMFISIS density, and the HOPE partial density for electrons >200 eV. Over the density bump, the total pressure remained approximately the same, where the decreased magnetic pressure was balanced primarily by the increased electron thermal pressure (Panel e). Consequently, the plasma beta increased to 1.5 from the background value of 1 (Panel f).

To explain the local density increase and the reappearance of plasma cloak around 02:09 to 02:10 UT (Figure 1), we argue that there was a spatial protrusion of plasmapause and the associated cloak, because similar cloak signatures are seen in the previous orbit (not shown). Table 1 listed the MHD flow velocity  $\vec{v}$ , which is the species average of the H+ and O+ bulk velocities obtained from the HOPE measurements. It contains a finite parallel component presumably related to the ion outflows, and its perpendicular components are primarily eastward and slightly outward. Such perpendicular components are expected if the plasma convection is around a protrusion. The protrusion decreased the distance of RBSP-A from the plasmapause, causing more electrons to be detected. From Figure 1e, we can see that around 00:00 and 08:00 UT, the outer boundary of the plasma cloak was about 1 Re outside of where the inner boundary of the plasma sheet and plasmapause touched. Based on the reappearing of the cloak around 02:00 UT and assuming the 1 Re distance, we suspect the plasmapause/inner boundary of the plasma sheet was around 4.6 Re. The fact that electron energy decreased to a minimum around 02:00 UT (Figure 1b) probably means that RBSP-A moved closer to the inner boundary of the plasma sheet, again suggesting there is a protrusion of the plasmapause.

#### 4. Discussion

In this event, RBSP-A observed significant Poynting flux around 02:09 to 02:10 UT, when the auroral beads expanded over the local time of RBSP-A (Figure 2, Panels a and d), suggesting a spatial and temporal correlation and thus a conjunction between the auroral beads and RBSP-A. Note that the conjunction is determined purely based on the local time of RBSP-A and the azimuthally evolving aurora. No model-dependent mapping

TIAN ET AL 5 of 9

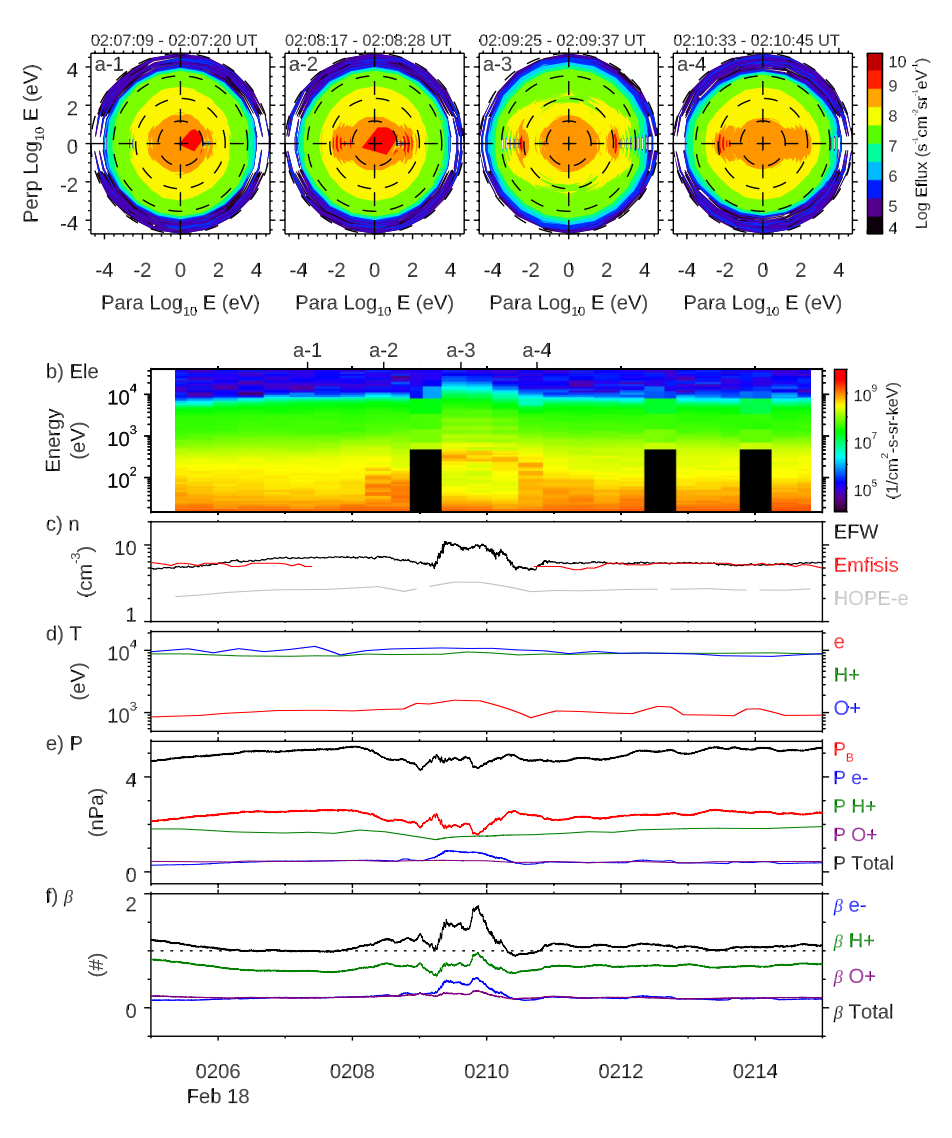


**Figure 3.** Thermal plasma measurements. Panels a-1 to a-4 show the electron pitch angle distribution. Each is a snapshot of the electron distribution over one spin of the spacecraft as a function of energy and direction relative to the background magnetic field. Panel b shows the electron energy-time spectrogram, Panel c shows the plasma density derived from EFW (black) and EMFISIS (red), and the partial electron density (>200 eV) derived from HOPE (gray). Panel d shows the temperature of the electron and ion (assuming only H+ and O+). Panel e shows the magnetic pressure and the thermal pressures of e-, H+, and O+, and the total pressure (magnetic plus thermal). Panel f shows the partial plasma beta (up to 50 keV). The conjunction around 02:09 to 02:10 UT was associated with electron beams of 100–400 eV (Panels a-2 to a-4 and Panel b), electron density increase (Panels c), and beta increase (Panel f).

is involved. To further study the role of KAW as the auroral acceleration mechanism for the auroral beads, we discuss the relation between the KAWs and beads in our event, investigate the relationship between the KAWs and electron beams at RBSP-A, and then estimate the wave-particle interaction along the field line from RBSP-A down to the ionosphere.

# 4.1. KAWs and the Source Region of Beading

Auroral beads are known to develop in both hemispheres with remarkable similarities (Motoba et al., 2012), suggesting a common source region around the equator. Observations in this event suggest that RBSP-A was along the source region magnetic field lines for the following reasons. The observed Poynting fluxes were toward the southern hemisphere. They should result in auroral beads in the southern hemisphere similar to those captured by the GBAY all-sky imager in the northern hemisphere, because the Poynting fluxes exceeded the threshold for

TIAN ET AL 6 of 9



powering visible aurora (1 mW/m²) and because they are an important energy source for electron acceleration responsible for dynamic aurora (Keiling et al., 2003; Tian et al., 2021; Wygant et al., 2000). The fact that the Poynting fluxes were southward means that the Alfvén waves and KAWs were generated northward of RBSP-A and that similar Poynting fluxes should be emitted toward the northern ionosphere. Based on Poynting flux and beading observations, we conjecture that KAWs are generated within the source region for auroral beads and propagate along field lines toward both hemispheres.

Assuming that RBSP-A was within or close to the source region of beading, our observations provide interesting indications for beading instabilities. The local plasma beta was 1–1.5, primarily because RBSP-A was only 5.6 Re away from the Earth, where the magnetic pressure is still significant. Considering that RBSP-A was below the magnetic equator and that the magnetic field may be locally stretched, the beta at the equator may be higher, but unlikely to be an order of magnitude larger. Therefore our observations do not favor instabilities that require a high beta, for example, the kinetic ballooning instability (Cheng & Lui, 1998) and cross-field current instability (Lui et al., 1991). For this particular event, shear flow ballooning instability (Viñas & Madden, 1986; Voronkov et al., 1997) and kinetic ballooning interchange instability (Pritchett & Coroniti, 2010), which do not require high beta to grow, thus may be feasible for the observed plasma condition. As mentioned in Section 3, RBSP-A was estimated to be within 1 Re outside where the plasmapause and plasma sheet touched. This means that the beading source region is very close to the inner edge of the plasma sheet. However, the kinetic ballooning interchange instability is suggested to occur outside the  $B_z$  minimum and thus in the mid-tail (Pritchett & Coroniti, 2010). Therefore, among the commonly suggested instabilities, our observations favor the shear flow ballooning instability for this beading event.

The availability of wave observations around the source region allows us to directly compare these observations to those of the auroral beads. For example, around the conjunction, the auroral beads propagated eastward at the angular speed of 1.9 deg/min (Figure 2a). This value scales to 20 km/s at RBSP-A (5.6 Re), coinciding with the eastward flow speed from HOPE (Table 1). This speed match is consistent with the recent observations on beading motion being related to plasma convection (Nishimura et al., 2022). This may also be related to the observations showing that the ballooning mode wave has almost zero frequency in the plasma frame (Saito et al., 2008). It is interesting to investigate how instability associated with beading may be related to the generation of the observed Alfvén waves, but a possible mechanism is through the flow shear of the azimuthal plasma convection. The Alfvén waves then cascade into the observed KAWs through phase mixing (Wright et al., 1999). For example, the large KAWs were seen around 02:09:20 and 02:10:10 UT (Figure 2 Panels b and c). These times coincided with density gradients (Figure 3b) where phase mixing tends to occur.

# 4.2. Local Alfvénic Acceleration

The electron beams at 100–400 eV observed at RBSP-A are interpreted as the local acceleration signature of the KAWs. The reappearing of the cloak (Figure 1c) suggests that RBSP-A moved closer to the plasmapause and could access the electrons of plasmaspheric origin. Although the plasma sheet electrons are 1 keV, the plasmaspheric electrons are of much lower temperature yet high in number density. Assuming a nominal temperature of 20 eV, the corresponding thermal speed  $v_{Te}$  is 5.5  $v_A$ . Therefore the Landau resonance applies to the core of the electron distribution through weak nonlinear Landau resonance (An et al., 2021).

In the regime of Landau resonance, the electrons with velocity in  $v_A \pm v_{tr}$  can be trapped by KAW, where  $v_{tr} = \sqrt{2e\delta\phi/m_e}$  is the trapping velocity and  $\delta\phi$  is the wave electric potential along the field line (An et al., 2021; Wygant et al., 2002). In this event, the MLat of RBSP-A was -0.4 deg, or 250 km off the equator. Using this distance and  $E_{\parallel} = 1$  mV/m, we have  $\delta\phi = 250$  V and  $v_{tr} \gg v_A$ . Here we estimate  $E_{\parallel} = \rho^2 k_{\parallel} k_{\perp} E_{\perp}$  following (Lysak, 1990), where  $\rho$  is the ion acoustic gyroradius, and use  $\rho k_{\perp} \sim 1$  and  $E_{\perp} \sim 15$  mV/m from our observations and the typical value of  $k_{\perp}/k_{\parallel} = 15$ . The upper bound of electron energy due to local KAW acceleration can be estimated as  $E_{\rm max} = m_e v_{tr}^2/2 = 2e\delta\phi = 500$  eV. According to this estimation, Alfvénic acceleration within or close to the source region can produce the observed electron beams of several 100 eV.

# 4.3. Further Alfvénic Acceleration at Lower Altitudes

Low-altitude observations show that auroral beads are in conjunction with keV electrons (Motoba & Hira-hara, 2016). This means that further acceleration occurs along the flux tube from the source region to the ionosphere. Many acceleration mechanisms through Alfvén waves have been numerically simulated (Artemyev

TIAN ET AL 7 of 9



et al., 2015; Damiano et al., 2018; Schroeder et al., 2021; Watt & Rankin, 2010). In addition, electron beams of 1–2 keV that are accelerated by KAWs have been observed off the equator (Wygant et al., 2002). Here  $v_{Te}/v_A$  is the key parameter controlling Alfvénic acceleration, where  $v_{Te}$  is the electron thermal speed and  $v_A$  is the Alfvén speed.

Based on the estimated altitude profile of  $v_{Te}/v_A$  from Schroeder et al. (2021),  $v_{Te}/v_A \in (0.1, 10)$  above the distance of ~3 Re, or the altitude of ~2 Re. As the Alfvén waves propagate toward the ionosphere, it is very likely that further Alfvénic acceleration occurs in this altitude range. For KAWs, An et al. (2021) demonstrated Alfvénic acceleration on electrons at  $v_{Te}/v_A$  at 2 and 4 through PIC simulations. For inertial Alfvén waves, Schroeder et al. (2021) demonstrated Alfvénic accelerated electron beams in lab plasmas at  $v_{Te}/v_A \sim 0.3$ . Based on these simulations and observations, it is clear that the 100–400 eV electron beams will be further accelerated by Alfvén waves at lower altitudes, and that Alfvénic acceleration can produce keV electrons as demonstrated in simulations (Artemyev et al., 2015; Damiano et al., 2018; Schroeder et al., 2021; Watt & Rankin, 2010) and observations (Wygant et al., 2002).

## 5. Conclusions

We have studied a fortuitous conjunction event between auroral beads and KAWs observed around the equator at the distance of 5.6 Re. The conjunction is inferred based on the fact that the KAWs were observed around the time when the auroral beads developed over the local time of RBSP-A. Observations at the spacecraft show electron beams of 100–400 eV, which is a typical signature of local Alfvénic acceleration. The Poynting flux associated with Alfvén waves and KAWs was of a plausible magnitude to power the auroral beads. The comparison between the Alfvén speed and electron thermal speed at different altitudes shows that further Alfvénic acceleration is likely to occur to at least the altitude of 2 Re.

These observations suggest that KAWs are generated around the equator and propagate into the northern and southern hemispheres. Alfvénic acceleration is likely to be the acceleration mechanism for auroral beads. Specifically, KAWs accelerate local cold electrons around the plasmapause to several 100 eV around the equator. These electrons may be further accelerated ~1 keV off the equator by either kinetic or inertial Alfvén waves. The keV electrons directly account for the auroral beads.

# **Data Availability Statement**

We thank the following spacecraft mission and relevant instrument teams for providing the data used in this study, including the THEMIS all-sky imagers, the EMFISIS, EFW, and HOPE instrument onboard RBSP. The data used in this study are available online. THEMIS all-sky imager data are available at https://cdaweb.gsfc.nasa.gov/pub/data/themis/. RBSP data are available at https://cdaweb.gsfc.nasa.gov/pub/data/rbsp/.

## References

Akasofu, S.-I. (1964). The development of the auroral substorm. Planetary and Space Science, 12(4), 273–282. https://doi.org/10.1016/0032-0633(64)90151-5

An, X., Bortnik, J., & Zhang, X.-J. (2021). Nonlinear Landau resonant interaction between kinetic Alfvén waves and thermal electrons: Excitation of time domain structures. *Journal of Geophysical Research: Space Physics*, 126(1), e2020JA028643. https://doi.org/10.1029/2020ja028643

Artemyev, A. V., Rankin, R., & Blanco, M. (2015). Electron trapping and acceleration by kinetic Alfven waves in the inner magnetosphere. *Journal of Geophysical Research: Space Physics*, 120(12), 10305306–10306310. https://doi.org/10.1002/2015ja021781

Chappell, C. R. (1982). Low energy particles in the magnetosphere. Advances in Space Research, 2(1), 33–38. https://doi.org/10.1016/0273-1177(82)90089-8

Chaston, C. C., Bonnell, J. W., & Salem, C. (2014). Heating of the plasma sheet by broadband electromagnetic waves. *Geophysical Research Letters*, 41(23), 8185–8192. https://doi.org/10.1002/2014GL062116

Cheng, C. Z., & Lui, A. T. Y. (1998). Kinetic ballooning instability for substorm onset and current disruption observed by AMPTE/CCE. Geophysical Research Letters, 25(21), 4091–4094. https://doi.org/10.1029/1998gl900093

Damiano, P. A., Chaston, C. C., Hull, A. J., & Johnson, J. R. (2018). Electron distributions in kinetic scale field line resonances: A comparison of simulations and observations. *Geophysical Research Letters*, 45(12), 5826–5835. https://doi.org/10.1029/2018g1077748

Donovan, E., Mende, S., Jackel, B., Frey, H., Syrjäsuo, M., Voronkov, I., et al. (2006). The THEMIS all-sky imaging array—System design and initial results from the prototype imager. *Journal of Atmospheric and Solar-Terrestrial Physics*, 68(13), 1472–1487. https://doi.org/10.1016/j.jastp.2005.03.027

Elphinstone, R. D., Hearn, D. J., Cogger, L. L., Murphree, J. S., Singer, H., Sergeev, V., et al. (1995). Observations in the vicinity of substorm onset: Implications for the substorm process. *Journal of Geophysical Research*, 100(A5), 7937–7969. https://doi.org/10.1029/94ja02938

#### Acknowledgments

The authors thank the following funding sources, including the NSF Grant 2108582, NASA grants 80NSSC19K0306, 80NSSC20K1314, 80NSSC20K1269, and NASA prime contract NAS5-01072.

TIAN ET AL 8 of 9



- Funsten, H. O., Skoug, R. M., Guthrie, A. A., MacDonald, E. A., Baldonado, J. R., Harper, R. W., et al. (2013). Helium, oxygen, proton, and electron (HOPE) mass spectrometer for the radiation belt storm probes mission. Space Science Reviews, 179, 1–484. https://doi.org/10.1007/s11214-013-9968-7
- Génot, V., Louarn, P., & Mottez, F. (2004). Alfvén wave interaction with inhomogeneous plasmas: Acceleration and energy cascade towards small-scales. Annales Geophysicae, 22(6), 2081–2096. https://doi.org/10.5194/angeo-22-2081-2004
- Henderson, M. G. (1994). *Implications of Viking imager results for substorm models*. Doctoral dissertation, University of Calgary (Canada). https://doi.org/10.11575/PRISM/22487
- Henderson, M. G. (2009). Observational evidence for an inside-out substorm onset scenario. Annales Geophysicae, 27(5), 2129–2140. https://doi.org/10.5194/angeo-27-2129-2009
- Kalmoni, N. M. E., Rae, I. J., Murphy, K. R., Forsyth, C., Watt, C. E. J., & Owen, C. J. (2017). Statistical azimuthal structuring of the substorm onset arc: Implications for the onset mechanism. Geophysical Research Letters, 44(5), 2078–2087. https://doi.org/10.1002/2016gl071826
- Kalmoni, N. M. E., Rae, I. J., Watt, C. E. J., Murphy, K. R., Forsyth, C., & Owen, C. J. (2015). Statistical characterization of the growth and spatial scales of the substorm onset arc. *Journal of Geophysical Research: Space Physics*, 120(10), 8503–8516. https://doi.org/10.1002/2015ja021470
- Kalmoni, N. M. E., Rae, I. J., Watt, C. E. J., Murphy, K. R., Samara, M., Michell, R. G., et al. (2018). A diagnosis of the plasma waves responsible for the explosive energy release of substorm onset. *Nature Communications*, 9(1), 4806. https://doi.org/10.1038/s41467-018-07086-0
- Keiling, A., Wygant, J. R., Cattell, C. A., Mozer, F. S., & Russell, C. T. (2003). The global morphology of wave poynting flux: Powering the aurora. Science, 299(5605), 383–386. https://doi.org/10.1126/science.1080073
- Kletzing, C. A., Kurth, W. S., Acuna, M., MacDowall, R. J., Torbert, R. B., Averkamp, T., et al. (2013). The electric and magnetic field instrument suite and Integrated science (EMFISIS) on RBSP. Space Science Reviews, 179(1), 127–181. https://doi.org/10.1007/s11214-013-9993-6
- Liang, J., Donovan, E. F., Liu, W. W., Jackel, B., Syrjäsuo, M., Mende, S. B., & Connors, M. (2008). Intensification of preexisting auroral arc at substorm expansion phase onset: Wave-like disruption during the first tens of seconds. *Geophysical Research Letters*, 35(17). https://doi. org/10.1029/2008g1033666
- Lui, A. T. Y., Chang, C.-L., Mankofsky, A., Wong, H.-K., & Winske, D. (1991). A cross-field current instability for substorm expansions. *Journal of Geophysical Research*, 96(A7), 11389–11401. https://doi.org/10.1029/91ja00892
- Lysak, R. L. (1990). Electrodynamic coupling of the magnetosphere and ionosphere. Space Science Reviews, 52(1-2), 33-87. https://doi.org/10.1007/BF00704239
- Lysak, R. L., & Lotko, W. (1996). On the kinetic dispersion relation for shear Alfvén waves. Journal of Geophysical Research, 101(A3), 5085–5094. https://doi.org/10.1029/95JA03712
- Mende, S. B., Harris, S. E., Frey, H. U., Angelopoulos, V., Russell, C. T., Donovan, E., et al. (2008). The THEMIS array of ground-based observatories for the study of auroral substorms. Space Science Reviews, 141(1), 357–387. https://doi.org/10.1007/s11214-008-9380-x
- Motoba, T., & Hirahara, M. (2016). High-resolution auroral acceleration signatures within a highly dynamic onset arc. *Geophysical Research Letters*, 43(5), 1793–1801. https://doi.org/10.1002/2015g1067580
- Motoba, T., Hosokawa, K., Kadokura, A., & Sato, N. (2012). Magnetic conjugacy of northern and southern auroral beads. *Geophysical Research Letters*, 39(8). https://doi.org/10.1029/2012gl051599
- Nishimura, Y., Artemyev, A. V., Lyons, L. R., Gabrielse, C., Donovan, E. F., & Angelopoulos, V. (2022). Space-ground observations of dynamics of substorm onset beads. *Journal of Geophysical Research: Space Physics*, 127(2), e2021JA030004. https://doi.org/10.1029/2021ja030004
- Nishimura, Y., Yang, J., Pritchett, P. L., Coroniti, F. V., Donovan, E. F., Lyons, L. R., et al. (2016). Statistical properties of substorm auroral onset beads/rays. *Journal of Geophysical Research: Space Physics*, 121(9), 8661–8676. https://doi.org/10.1002/2016ja022801
- Panov, E. V., Baumjohann, W., Nakamura, R., Pritchett, P. L., Weygand, J. M., & Kubyshkina, M. V. (2019). Ionospheric footprints of detached magnetotail interchange heads. Geophysical Research Letters, 46(13), 7237–7247. https://doi.org/10.1029/2019gl083070
- Pritchett, P. L., & Coroniti, F. V. (2010). A kinetic ballooning/interchange instability in the magnetotail. *Journal of Geophysical Research*, 115(A6). https://doi.org/10.1029/2009ja014752
- Rae, I. J., & Watt, C. E. J. (2016). ULF waves above the nightside auroral oval during substorm onset. *Low-frequency waves in space plasmas* (pp. 99–120). American Geophysical Union (AGU). https://doi.org/10.1002/9781119055006.ch7
- Rae, I. J., Watt, C. E. J., Mann, I. R., Murphy, K. R., Samson, J. C., Kabin, K., & Angelopoulos, V. (2010). Optical characterization of the growth and spatial structure of a substorm onset arc. *Journal of Geophysical Research*, 115(A10). https://doi.org/10.1029/2010ja015376
- Saito, M. H., Miyashita, Y., Fujimoto, M., Shinohara, I., Saito, Y., Liou, K., & Mukai, T. (2008). Ballooning mode waves prior to substorm-associated dipolarizations: Geotail observations. *Geophysical Research Letters*, 35(7). https://doi.org/10.1029/2008gl033269
- Schroeder, J. W. R., Howes, G. G., Kletzing, C. A., Skiff, F., Carter, T. A., Vincena, S., & Dorfman, S. (2021). Laboratory measurements of the physics of auroral electron acceleration by Alfvén waves. *Nature Communications*, 12(1), 3103. https://doi.org/10.1038/s41467-021-23377-5
- Tian, S., Colpitts, C. A., Wygant, J. R., Cattell, C. A., Ferradas, C. P., Igl, A. B., & Donovan, E. F. (2021). Evidence of Alfvenic Poynting flux as the primary driver of auroral motion during a geomagnetic substorm. *Journal of Geophysical Research: Space Physics*, 126(5), e2020JA029019. https://doi.org/10.1029/2020ja029019
- Viñas, A. F., & Madden, T. R. (1986). Shear flow-ballooning instability as a possible mechanism for hydromagnetic fluctuations. *Journal of Geophysical Research*, 91(A2), 1519–1528. https://doi.org/10.1029/ja091ia02p01519
- Voronkov, I., Rankin, R., Frycz, P., Tikhonchuk, V. T., & Samson, J. C. (1997). Coupling of shear flow and pressure gradient instabilities. *Journal of Geophysical Research*, 102(A5), 9639–9650. https://doi.org/10.1029/97ja00386
- Watt, C. E. J., & Rankin, R. (2010). Do magnetospheric shear Alfvén waves generate sufficient electron energy flux to power the aurora? *Journal of Geophysical Research*, 115(A7). https://doi.org/10.1029/2009JA015185
- Wright, A. N., Allan, W., Elphinstone, R. D., & Cogger, L. L. (1999). Phase mixing and phase motion of Alfvén waves on tail-like and dipole-like magnetic field lines. *Journal of Geophysical Research*, 104(A5), 10159–10175. https://doi.org/10.1029/1999ja900018
- Wygant, J. R., Bonnell, J. W., Goetz, K., Ergun, R. E., Mozer, F. S., Bale, S. D., et al. (2013). The electric field and waves instruments on the radiation belt storm probes mission. *Space Science Reviews*, 179(1), 183–220. https://doi.org/10.1007/s11214-013-0013-7
- Wygant, J. R., Keiling, A., Cattell, C. A., Johnson, M., Lysak, R. L., Temerin, M., et al. (2000). Polar spacecraft based comparisons of intense electric fields and Poynting flux near and within the plasma sheet-tail lobe boundary to UVI images: An energy source for the aurora. *Journal of Geophysical Research*, 105(A8), 18675–18692. https://doi.org/10.1029/1999JA900500
- Wygant, J. R., Keiling, A., Cattell, C. A., Lysak, R. L., Temerin, M., Mozer, F. S., et al. (2002). Evidence for kinetic Alfvén waves and parallel electron energization at 4-6 RE altitudes in the plasma sheet boundary layer. *Journal of Geophysical Research*, 107(A8), 1201–1. https://doi.org/10.1029/2001JA900113
- Xing, X., Wang, C.-P., Liang, J., & Yang, B. (2020). Ballooning instability in the plasma sheet transitionregion in conjunction with nonsubstorm auroral wave structures. *Journal of Geophysical Research: Space Physics*, 125(3), e2019JA027340. https://doi.org/10.1029/2019ja027340

TIAN ET AL 9 of 9